WILEY | Hindawi

Research Article

Enhanced Second-Order Sliding Mode Control Technique for a Five-Phase Induction Motor

Mahmoud A. Mossa [ID],[1] **Hamdi Echeikh** [ID],[2] **Najib El Ouanjli** [ID],[3]
and Hassan Haes Alhelou [ID][4]

[1]*Electrical Engineering Department, Faculty of Engineering, Minia University, Minia 61111, Egypt*
[2]*Electrical Engineering Department, National Engineering School of Monastir, Monastir, Tunisia*
[3]*LMIET, Hassan First University, Settat, Morocco*
[4]*Department of Electrical Power Engineering, Tishreen University, 2230 Lattakia, Syria*

Correspondence should be addressed to Mahmoud A. Mossa; mahmoud_a_mossa@mu.edu.eg and Hassan Haes Alhelou;
h.haesalhelou@gmail.com

Recently, several research papers have addressed multiphase induction motor (IM) drives, owing to their several benefits compared to the three-phase motors, including increasing the torque pulsations frequency and reducing the rotor harmonic current losses. Thus, designing a robust controller to ensure the proper operation of such motors became a challenge. The present study reports the design of an effective second-order sliding mode control (SO-SMC) approach for a five-phase IM drive. The proposed control approach finds its strongest justification for the problem of using a law of nonlinear control robust to the system uncertainties of the model without affecting the system's simplicity. The formulation of the proposed SO-SMC approach is a prescribed process to ensure the stability and proper dynamics of the five-phase IM. A detailed stability analysis is also presented for this purpose. To validate the effectiveness of the proposed controller, the five-phase IM drive is tested under different dynamic situations, including load changes and system uncertainties. The presented numerical results prove the ability of the designed SO-SMC to handle high system nonlinearities and maintain high robustness against uncertainties.

1. Introduction

The control of electric machines always raises the interest of the scientific communities. This is due to the diversity of industrial applications requiring speed, torque, or position control. Starting with the continuous current machine (DC), the evolutionary trend took place in the 80s towards the direction of substituting this machine by that with alternating current (AC). Therefore, the three-phase machine associated with a static converter constituted a variator whose use is largely present in the industrial sector. This interest has arisen on the one hand thanks to the development of power electronics and on the other hand thanks to the technical and economic advantages offered by this machine compared to the DC machine [1]. Nevertheless, the three-phase electric actuator remains restricted to the lower limit of the range of high power up to a few megawatts due to the electrical stresses experienced by the semiconductors.

Thus, for applications requiring a higher level of power, a segmentation of the power by multiplication of the number of machine phases is necessary. Indeed, the distribution of the power in a number of phases greater than three helped significantly in handling high-power applications, and this solution resulted in what is known as "multiphase machines."

Even though the conception of variable speed multiphase machines drives dates from the 1960s, the multiphase actuators were not seriously utilized in the industry until the mid-1990s. The industrial applications include the propulsion systems of ships, traction locomotives, hybrid and electric vehicles, avionics, and industrial applications of high power. As a result, there has been an escalating interest in these systems around the world, resulting in a massive research work over the past decade [2–16]. In comparison with conventional three-phase machines, multiphase machines have exceptional outstanding features. Firstly, the increase in

the number of phases makes it possible to reduce electromagnetic torque ripples [17, 18]. Multiphase machines are as a result an attractive selection for demanding applications in respect of acoustic or vibratory discretion. Then, the multiplication of the number of phases increases the possibilities of functioning in degraded (faulty) mode while preserving an acceptable quality of torque in terms of ripples and amplitude. This problem is fundamental for applications that guarantee excellent continuity of service [19–21]. Indeed, the treatment resulting from the degradation of the power supply of the three-phase machines requires material modifications, which must be reduced to the minimum to ensure the continuation of operation at a minimum cost. Nevertheless, the approach is different when choosing and using polyphase machines.

Indeed, the continuation of operation for these machines in degraded mode goes through a control strategy taking into account additional degrees of freedom without the need to add additional equipment. In addition, a structure with a large number of phases means power segmentation, which decreases the rating constraints on the power electronics units supplying each phase. This is why multiphase machines are used in very high-power applications [22, 23]. In addition, the complementary degrees of freedom available for multiphase machines are utilized for torque production. In other words, these extra degrees of freedom can be exploited to provide improvements in torque production through the injection of high-order current harmonics. They also allow the inverter to drive multiple multiphase motors simultaneously. As a result, multiphase drives are becoming more common in certain variable speed utilizations, such as marine, avionics, automotive, and railroad traction [24, 25].

In the formulation of any control problem, there are typical anomalies between the real system and the mathematical model developed for the control design. This distinction may be due to the variation of the parameters of the system dynamics or to the approximation of the complex system behavior by a model. This has led to intense interest in developing robust control methods that seek to address this problem. The most known control strategy of the machine is the flux-oriented control [26, 27]. The FOC is a control algorithm that is based on integral proportional action. The FOC control may be sufficient if the requirements on the accuracy and performance of the system are not too strict. Nevertheless, in the opposite case and particularly when the ordered part is subjected to strong nonlinearities and to temporal variations, it is necessary to design control algorithms ensuring the robustness of the behavior of the process vis-à-vis the uncertainties on the parameters and their variations. Since the simple PI regulator presents insufficient performance for AC current regulation, several control techniques using different approaches were proposed in the literature. Several nonlinear state feedback strategies, especially sliding mode control (SMC), eventually are an interesting substitution to the FOC technique for three-phase motor drives to carry out great achievements [28]. This strategy has been extensively adapted to the traditional three-phase motor drives justifying diverse attractive lineaments in comparison with the traditional FOC.

The main prosperities of SMC are its robustness in case of parameter uncertainties and disturbance. This strategy of control attempts great stability performance and very fast dynamic response [29]. Nonetheless, the chattering phenomenon of the SMC remains the main limitation of such a technique, which has been exposed in several studies [30, 31]. The study in [30] proposed an adaptive SMC based on recurrent RBFN applied to an induction motor servo drive to decrease the chattering generated by the estimation of the unmodeled uncertainties. In [29], an adaptive control is developed to change the saturation function to avoid the chattering issue. In [31], an original adaptive SMC is presented to obtain a synchronized control algorithm for several PMSMs, which shows promising results in the point of view of decreasing the chattering problem and high-performance control.

Different control strategies for multiphase machines and specially five-phase induction motors have been applied as an illustration of the two recognized control methods of the FOC [32] and the direct torque control (DTC) [16, 33–35], owing to their simple implementation. Nonetheless, the considerable inconvenience of these strategies of control is their notable sensitivity due to the existence of torque ripples and the change of motor parameters. Several researches can be found in the literature dealing with those methods. The study in [36] proposed indirect rotor flux-oriented control of an FPIM with novel rotor resistance estimation utilizing a sliding mode estimator to avoid the effects that come from the rotor resistance variation. Also, the same authors presented in [37] an adaptive DTC using sliding mode-Luenberger observer for online stator resistance observation for FPIM drives to overcome the stator resistance variation for DTC. Moreover, it is well-known that the nonlinear control is less sensitive against the system parameters; however, few researchers applied a nonlinear technique to a multiphase machine. In [38], the authors proposed a nonlinear backstepping control of FPIM drive at low-speed conditions, and it was verified through the experimental implementation.

In [39], a backstepping strategy articulated on space vector pulse width modulation (SVPWM) is developed. This utilization associates the proposed control strategy with the presented motor method. The presented control strategy gives an admirable performance and a rapid speed tracking response. Additionally, it carries out some key improvements like the enhancement of the robustness to the inevitable motor parameters variation, which aid first in enhancing the dynamic performance of the motor and second in decreasing the torque ripples. However, designing a robust controller for the five-phase IMs and testing their ability to encounter the parameters change without incorporating adaptive observers are quite rare, and for this reason, the present paper introduces an analytical study of a new adaptive SMC for a sinusoidal winding distribution five-phase IM. The essential improvement of this paper is the design of an adaptive second-order SMC of a five-phase IM through which the shortages in classic SMC are avoided, and the system robustness is effectively enhanced.
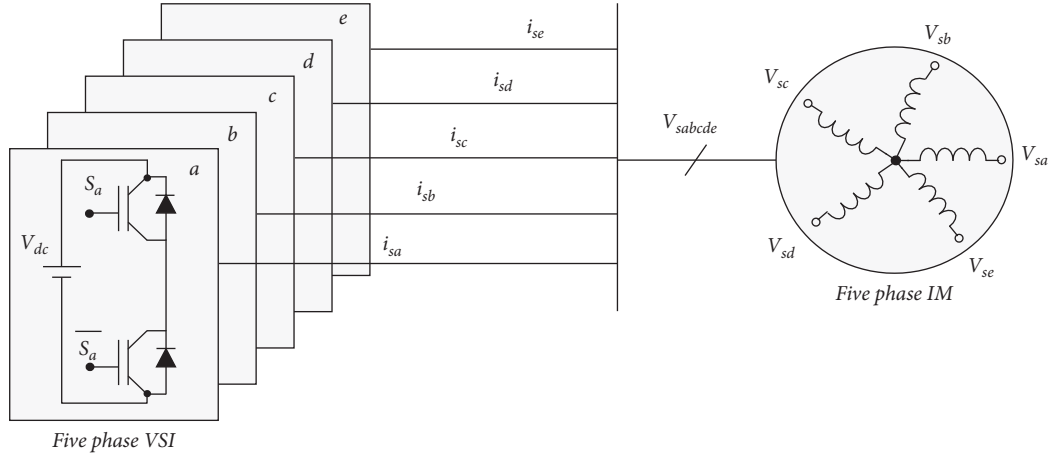
Figure 1: Configuration of five-phase IM drive system.

The study contributions can be itemized as follows:

(i) A robust adaptive second-order sliding mode control is designed and analyzed in order to ensure the robustness of a five-phase IM drive system against uncertainties and load disturbance as well.

(ii) The design procedure is accomplished in a systematic manner in order to visualize the base principle of the controller.

(iii) Different from the control approaches, which considered the sliding mode theory to only design one or two control loops (i.e., speed and flux) and used a PI controller for the remaining loops (i.e., current), the proposed SO-SMC considers designing all control loops together.

(iv) The proposed SMC control system is considered an effective tool for handling high nonlinearities.

(v) The validation of the proposed SMC system is achieved using extensive evaluation tests.

The structure of the paper is formulated as follows: Section 2 introduces the model of FPIM. Then, Section 3 presents the design of a novel method to determine the current references, respectively, for the d-q and w-u planes. The voltage references for both planes d-q and w-u are also determined in Section 4. The evaluation results are introduced and discussed in Section 5. Meanwhile, Section 6 is dedicated to the research outcomes.

2. Modeling of Five-Phase IM

A layout of the drive system utilized in this paper is shown in Figure 1. The system is formed by an FPIM of a two-level IGBT-established power converter. In the first step, the modeling equations taking account a distributed winding five-phase IM are defined, and the phase variables model is described [17]. The model is evaluated in the (α-β, x-y) stator frame adopting the Concordia transformation. Then, for control purposes, the model needs to be inspected in the (d-q, w-u) rotating frame, investigating the Park transformation.

The FPIM under study consists of a stator with five windings which are uniformly distributed over the circumference of the stator with an electrical displacement of $v = 2\pi/5$; meanwhile, the rotor has a squirrel-cage structure. Two different methods can be contemplated in the time of modeling an electrical motor, particularly the vector space decomposition algorithm and phase variable modeling. The motor reluctance is independent of the rotor position, the motor is composed of identical windings uniformly distributed over the rotor and the stator, and finally, the rotor has a squirrel-cage structure. Implementing Concordia and Park transformations given in [17], the model of five-phase IM in the (d, q, w, u) rotating frame with sinusoidal electromotive force under balanced circumstances is defined by the following equation:

$$\dot{\Omega} = \frac{B_m}{J_m}\Omega + \frac{pM}{L_r}\varphi i_{sq} - \frac{1}{J_m}T_L,$$

$$\dot{i}_{sd} = -\frac{R_t}{\sigma L_s}i_{sd} + \omega_s i_{sq} + \frac{\mu}{\sigma L_s T_r}\varphi + \frac{1}{\sigma L_s}V_{sd},$$

$$\dot{i}_{sq} = -\frac{R_t}{\sigma L_s}i_{sq} - \omega_s i_{sd} - \frac{\mu}{\sigma L_s}\omega\varphi + \frac{1}{\sigma L_s}V_{sq},$$

$$\dot{i}_{sw} = -\frac{1}{T_{ls}}i_{sw} + \frac{1}{L_{ls}}V_{sw},$$

$$\dot{i}_{su} = -\frac{1}{T_{ls}}i_{su} + \frac{1}{L_{ls}}V_{su},$$

$$\dot{\varphi} = \frac{M}{T_r}i_{sd} - \frac{1}{T_r}\varphi,$$

(1)

where i_{sd}, i_{sq}, i_{sw}, and i_{su} design, respectively, the stator currents in the (d, q, w, u) rotating frame, Ω is the mechanical speed of the five-phase IM, T_L represents the load torque; meanwhile, the developed torque considering the flux orientation state is given by $T_{em} = (pM/L_r)\varphi i_{sq}$. p denotes the pole-pairs, and B_m and J_m are the friction and shaft momentum. $\omega = p\Omega$ designs the electrical motor speed, φ is the magnitude of the rotor flux, M denotes the

coupling inductance, L_s and L_r are the cyclic inductances, respectively, of the stator and rotor, L_{ls} presents the stator leakage inductance, and finally, V_{sd}, V_{sq}, V_{sw}, and V_{su} design, respectively, the stator voltage in the rotating (d, q, w, u) frame. In this rotating frame, the FPIM model can be projected in two different 2D coordinates, specifically $(d\text{-}q)$ and $(w\text{-}u)$, and one axis, namely, o, which presents zero relative components. Consequently, the model of FPIM represented by (1) can be rewritten by

$$
\begin{aligned}
\dot{\Omega} &= a_\omega \Omega + b_\omega \varphi i_{sq} - c_\omega T_L, \\
\dot{i}_{sd} &= a_d i_{sd} + \omega_s i_{sq} + b_d \varphi + d_d V_{sd}, \\
\dot{i}_{sq} &= a_d i_{sq} - \omega_s i_{sd} + c_d \omega \varphi + d_d V_{sq}, \\
\dot{i}_{sw} &= a_w i_{sw} + d_w V_{sw}, \\
\dot{i}_{su} &= a_w i_{su} + d_w V_{su}, \\
\dot{\varphi} &= a_\varphi i_{sd} - b_\varphi \varphi,
\end{aligned}
\tag{2}
$$

where

$$
\sigma = 1 - \frac{M^2}{L_s L_r},
$$

$$
R_t = \frac{1}{1 - T_s} + \frac{1 - \sigma}{\sigma T_r},
$$

$$
T_r = \frac{L_r}{R_r},
$$

$$
T_s = \frac{L_s}{R_s},
$$

$$
\mu = \frac{L_m}{L_r},
$$

$$
a_\omega = \frac{B_m}{J_m},
$$

$$
T_{ls} = \frac{L_{ls}}{R_s},
$$

$$
b_\omega = \frac{pM}{L_r},
$$

$$
c_\omega = \frac{1}{J_m},
$$

$$
a_d = -\frac{R_t}{\sigma L_s},
$$

$$
b_d = \frac{\mu}{\sigma L_s T_r},
$$

$$
d_d = \frac{1}{\sigma L_s},
$$

$$
c_d = -\frac{\mu}{\sigma L_s},
$$

$$
\begin{aligned}
a_w &= -\frac{1}{T_{ls}}, \\
d_w &= \frac{1}{L_{ls}}, \\
a_\varphi &= \frac{M}{T_r}, \\
b_\varphi &= \frac{1}{T_r}.
\end{aligned}
\tag{3}
$$

3. Design Procedure of the Proposed SO-SMC

3.1. Definition. The study of the sliding mode began in Yugoslavia in the 1960s, after this work was repeated elsewhere, either to complete the theoretical study or to study some possible applications. However, it is only in the 1980s that the sliding mode control has become interesting and attractive. It has been considered one of the control approaches for nonlinear systems and systems with inaccurate models. The theory of sliding mode systems is a nonlinear control mechanism featured by the interruption of control when passing through a switching surface called the sliding surface. The technique of sliding modes stands on moving the state trajectory of a system towards the sliding surface and making it switch with proper switching around it to the point of equilibrium. In general, the sliding control consists of two essential steps:

(i) Determining a state space area such that once the system is in that area, it has the required dynamic.

(ii) Derivation of a control law that drives the system to the specified state space area.

Figure 2 presents the sliding systems. The formulation of the SMC considers the problems of stability and appropriate performance in a systematic way in its procedure which is executed principally in three interrelated stages identified by the following:

(i) Selection of sliding surfaces.

(ii) Definition of the conditions of existence and convergence of the sliding regime.

(iii) Derivation of the control law.

The existence conditions and convergence are the criteria that permit the convergence of different system dynamics towards the sliding surface and to stay there independently of the perturbation. There are two categories of conditions which are as follows:

(i) It is presented and analyzed by Emilyanov and Utkin. It is a question of giving to the surface a dynamic convergent towards zero.

(ii) It is a question of choosing a candidate function of Lyapunov (positive scalar function) for the variables of state of the system and choosing a law of command which will decrease this function.
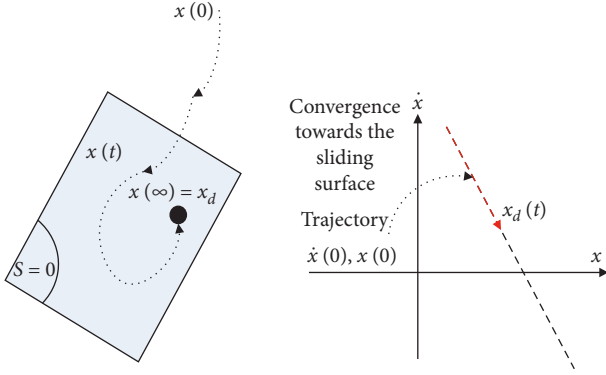
FIGURE 2: Sliding systems dynamics.

3.2. Design Steps.

The implementation of SMC on the three-phase motor is extensively presented and analyzed [25–27]. Nonetheless, concerning multiphase motor in the literature, one can find only a few works attending to it. In this situation, a novel SMC is designed to accomplish the control of FPIM in this section. The idea of the formulated SMC originated from the introduced definition of the sliding mechanism shown in Figure 2. In this effor, in the current study, the SMC is designed to obtain the control laws for managing speed, current and flux of five phase IM dissimilar to the control presented in [25], in which the SMC is applied only for speed control while using a PI controller for the current regulation. In the present study, one will simply apply the technique of adjustment by sliding mode to the five-phase IM, and we will establish the command value expressions based on the model established in the first section.

3.2.1. Design of Sliding Surface.

One can introduce the sliding surface in the R^2 state as follows:

$$S_k = h_k \cdot \left(c_k z_k + \int_0^t z_k(\tau) \cdot d\tau \right), \tag{4}$$

where z_k denotes the variable error for speed, current, and flux and the parameters c_k and h_k are two positive constants. In consideration that the control is adapted to five-phase IM, then six sliding surfaces are presented as follows:

$$S_1 = h_1 \left(c_1 z_1 + \int_0^t z_1(\tau) d\tau \right),$$

$$S_2 = h_2 \left(c_2 z_2 + \int_0^t z_2(\tau) d\tau \right). \tag{5}$$

$$S_3 = h_3 \left(c_3 z_3 + \int_0^t z_3(\tau) d\tau \right),$$

$$S_4 = h_4 \left(c_4 z_4 + \int_0^t z_4(\tau) d\tau \right). \tag{6}$$

$$S_5 = h_5 \left(c_5 z_5 + \int_0^t z_5(\tau) d\tau \right),$$

$$S_6 = h_6 \left(c_6 z_6 + \int_0^t z_6(\tau) d\tau \right), \tag{7}$$

where

$$z_1 = \Omega - \Omega^*,$$
$$z_2 = \varphi - \varphi^*,$$
$$z_3 = i_{sd} - i_{sd}^*,$$
$$z_4 = i_{sq} - i_{sq}^*,$$
$$z_5 = i_{sw} - i_{sw}^*,$$
$$z_6 = i_{su} - i_{su}^*, \tag{8}$$

where the symbol "*" is utilized to denote the reference value. c_k and h_k are positive constants and design the control parameters ($k = 1, 2, 3, 4, 5, 6$). z_1, z_2, z_3, z_4, z_5, and z_6 are presented as the tracking errors of speed, flux, d-current, q-current, w-current, and u-current, in turn.

3.2.2. Design of Control Law.

The application of the proposed SO-SMC is performed in three steps: speed control, flux control, and current control. When the sliding regime reaches the dynamics of the system, which is independent of the control law and which is intended to maintain the sliding conditions (the attractiveness of the surface), the surface can be determined independently of the order. Now, it remains to identify the reference required to pull the state trajectory towards the surface and then to its point of equilibrium while guaranteeing the conditions of existence of the sliding mode. In order to obtain the nominal model of the FPIM model, the nominal parameter values on the external disturbance should be considered. Accordingly, the model given by (2) of FPIM turns out to be

$$\dot{\Omega} = \bar{a}_\omega \Omega + \bar{b}_\omega \varphi i_{sq},$$
$$\dot{i}_{sd} = \bar{a}_d i_{sd} + \omega_s i_{sq} + \bar{b}_d \varphi + \bar{d}_d V_{sd},$$
$$\dot{i}_{sq} = \bar{a}_d i_{sq} - \omega_s i_{sd} + \bar{c}_d \omega \varphi + \bar{d}_d V_{sq},$$
$$\dot{i}_{sw} = \bar{a}_w i_{sw} + \bar{d}_w V_{sw},$$
$$\dot{i}_{su} = \bar{a}_w i_{su} + \bar{d}_w V_{su},$$
$$\dot{\varphi} = \bar{a}_\varphi i_{sd} - \bar{b}_\varphi \varphi, \tag{9}$$

where $\bar{a}_\omega$, $\bar{b}_\omega$, $\bar{a}_d$, $\bar{b}_d$, $\bar{c}_d$, $\bar{d}_d$, $\bar{a}_w$, $\bar{d}_w$, $\bar{a}_\varphi$, and $\bar{b}_\varphi$ present the nominal values, respectively, of a_ω, b_ω, a_d, b_d, c_d, d_d, a_w, d_w, a_φ, and b_φ. Taking into consideration the parameters variation, external load disturbance, and unexpected uncertainties, the FPIM model can be modeled as follows:

$$\dot{\Omega} = \left(\overline{a}_\omega + \Delta a_\omega\right)\Omega + \left(\overline{b}_\omega \Delta b_\omega\right)\varphi i_{sq}$$
$$+ c_\omega T_L + \delta_1,$$

$$i_{sd}^{\cdot} = \left(\overline{a}_d + \Delta a_d\right)i_{sd} + \omega_s i_{sq}$$
$$+ \left(\overline{b}_d + \Delta b_d\right)\varphi + \left(\overline{d}_d + \Delta d_d\right)V_{sd} + \delta_2,$$

$$i_{sq}^{\cdot} = \left(\overline{a}_d + \Delta a_d\right)i_{sq} - \omega_s i_{sd} + \left(\overline{c}_d + \Delta c_d\right)\omega\varphi \qquad (10)$$
$$+ \left(\overline{d}_d + \Delta d_d\right)V_{sq} + \delta_3,$$

$$i_{sw}^{\cdot} = \left(\overline{a}_\omega + \Delta a_w\right)i_{sw} + \left(\overline{d}_w + \Delta d_w\right)V_{sw} + \delta_4,$$

$$i_{su}^{\cdot} = \left(\overline{a}_w + \Delta a_w\right)i_{su} + \left(\overline{d}_w + \Delta d_w\right)V_{su} + \delta_5,$$

$$\dot{\varphi} = \left(\overline{a}_\varphi + \Delta a_\varphi\right)i_{sd} - \left(\overline{b}_\varphi + \Delta b_\varphi\right)\varphi + \delta_6.$$

Then, the expressions in (10) can be simplified as follows:

$$\dot{\Omega} = \overline{a}_\omega \Omega + \overline{b}_\omega \varphi i_{sq} + L_1,$$

$$i_{sd}^{\cdot} = \overline{a}_d i_{sd} + \omega_s i_{sq} + \overline{b}_d \varphi + \overline{d}_d V_{sd} + L_2,$$

$$i_{sq}^{\cdot} = \overline{a}_d i_{sq} - \omega_s i_{sd} + \overline{c}_d \omega\varphi + \overline{d}_d V_{sq} + L_3, \qquad (11)$$

$$i_{sw}^{\cdot} = \overline{a}_w i_{sw} + \overline{d}_w V_{sw} + L_4,$$

$$i_{su}^{\cdot} = \overline{a}_w i_{su} + \overline{d}_w V_{su} + L_5,$$

where

$$L_1 = a_\omega \Omega + b_\omega \varphi i_{sq} + c_\omega T_L + \delta_1,$$

$$L_2 = a_d i_{sd} + \omega_s i_{sq} + b_d \varphi + d_d V_{sd} + \delta_2,$$

$$L_3 = a_d i_{sq} - \omega_s i_{sd} + c_d \omega\varphi + d_d V_{sq} + \delta_3,$$
$$\qquad (12)$$
$$L_4 = a_w i_{sw} + d_w V_{sw} + \delta_4,$$

$$L_5 = a_w i_{su} + d_w V_{su} + \delta_5,$$

$$L_6 = a_\varphi i_{sd} - b_\varphi \varphi + \delta_6.$$

L_i ($i = 1, 2, 3, 4, 5, 6$) is the lumped uncertainty and pretended to be limited by $|L_i| < \chi_i$ ($i = 1, 2, 3, 4, 5, 6$), where χ_i is a positive constant.

(1) Speed Control Procedure. The speed error z_1 and its derivative $\dot{z}_1$ can be expressed by

$$z_1 = \Omega - \Omega^*, \qquad (13)$$

$$\dot{z}_1 = \dot{\Omega} - \dot{\Omega}^*. \qquad (14)$$

Using the first equality in (11), relation (14) can be expressed by

$$\dot{z}_1 = \overline{a}_\omega \Omega + \overline{b}_\omega \varphi i_{sq} + L_1 - \dot{\Omega}^*. \qquad (15)$$

The dynamic surface of the sliding mode of z_1 in the state R^2 is defined by

$$S_1 = h_1\left(c_1 z_1 + \int_0^t z_1(\tau)\mathrm{d}\tau\right). \qquad (16)$$

The differentiation of S_1 can then be expressed by

$$\dot{S}_1 = h_1\left(c_1 \dot{z}_1 + z_1\right). \qquad (17)$$

Replacing (15) with (17), the derivative of S_1 can be evaluated by

$$\dot{z}_1 = h_1\left(c_1\left(\overline{a}_\omega \Omega + \overline{b}_\omega \varphi i_{sq} + L_1 - \dot{\Omega}^*\right) + z_1\right). \qquad (18)$$

The desired performance can be achieved by solving (18) under a nominal machine model without taking into account the lumped uncertainties $L_1 = 0$ and $\dot{S}_1 = 0$.

$$i_{sqn}^* = -\left(c_1\overline{b}_\omega\right)^{-1} \cdot \left(\left(c_1\overline{b}_\omega + 1\right)z_1 + c_1\overline{a}_\omega\Omega^* - c_1\dot{\Omega}^*\right). \qquad (19)$$

In order to obtain a satisfactory performance of the control strategy against the uncertainties on the system dynamic system (lumped uncertainties), then a required discontinuous function named "reaching controller" needs to be joined to the control part to endure uncertainties beyond the sliding surface. Consequently, reaching control is defined by

$$i_{sqr}^* = -\left(\overline{b}_\omega \varphi\right)^{-1} \cdot k_1 \mathrm{sign}\left(S_1\right), \qquad (20)$$

where k_1 designs the switching gain. Thus, a relevant control of q-current considering uncertainties and unmodeled dynamics can be modeled by the following equation:

$$i_{sq}^* = i_{sqn}^* + i_{sqr}^*. \qquad (21)$$

By replacing (19) and (20) in (21), the command q-current component can be written as follows:

$$i_{sq}^* = -\left(c_1\overline{b}_\omega\right)^{-1} \cdot \left(\left(c_1\overline{a}_\omega + 1\right)z_1 + c_1\overline{a}_\omega\Omega^* - c_1\dot{\Omega}^*\right)$$
$$= -\left(\overline{b}_\omega \varphi\right)^{-1} \cdot k_1 \mathrm{sign}\left(S_1\right). \qquad (22)$$

(2) Flux Control Procedure. The flux error z_2 and its derivative $\dot{z}_2$ can be defined by

$$z_2 = \varphi - \varphi^*, \qquad (23)$$

$$\dot{z}_2 = \dot{\varphi} - \dot{\varphi}^* = \overline{a}_\varphi i_{sd} - \overline{b}_\varphi \varphi + L_6 - \dot{\varphi}^*. \qquad (24)$$

The dynamic surface of the sliding mode of z_2 in the state R^2 is itemized by

$$S_2 = h_2\left(c_2 z_2 + \int_0^t z_2(\tau)\mathrm{d}\tau\right). \qquad (25)$$

Setting (24) into (25), the derivative of S_2 can be formulated by

$$\dot{S}_2 = h_2\left(c_2\left(\overline{a}_\varphi i_{sd} - \overline{b}_\varphi \varphi + L_6 - \dot{\varphi}^*\right) + z_2\right). \qquad (26)$$

The desired performance can be obtained by solving (18) without contemplating the lumped uncertainties $L_6 = 0$ and $\dot{S}_2 = 0$. Then,

$$i_{sdn}^* = -\left(c_2\overline{b}_\varphi\right)^{-1} \cdot \left(\left(c_1\overline{b}_\varphi + 1\right)z_2 + c_2\overline{a}_\varphi \varphi^* - c_2\varphi^*\right). \qquad (27)$$

To get a satisfactory operation of the controller against the uncertainties in the system, then a reaching controller

needs to be combined with the control to handle these uncertainties beyond the sliding surface. Thus, the reaching control can be formulated by

$$i_{sdr}^* = -\left(\overline{b}_\varphi\right)^{-1} \cdot k_2 \mathrm{sign}\left(S_2\right), \qquad (28)$$

where k_2 designs the switching gain. Thus, a relevant control of d-current considering the uncertainties and unmodeled dynamics can be represented as follows:

$$i_{sd}^* = i_{sdn}^* + i_{sdr}^*. \qquad (29)$$

Substituting (27) and (28) into (29), the command q-current component can be written as follows:

$$i_{sd}^* = -\left(c_2 \overline{b}_\varphi\right)^{-1} \cdot \left(\left(c_1 \overline{b}_\varphi + 1\right)z_2 + c_2 \overline{a}_\varphi \varphi^* - c_2 \varphi^*\right)$$
$$-\left(\overline{b}_\varphi\right)^{-1} \cdot k_2 \mathrm{sign}\left(S_2\right). \qquad (30)$$

The reference w and u current components are controlled to be null for the five-phase induction motor in order to minimize the losses.

$$i_{sw}^* = i_{su}^* = 0.0. \qquad (31)$$

(3) Current Control Procedure. The derivatives of the (d-q-w-u) current deviations z_3, z_4, z_5, and z_6 are, respectively, presented as

$$\dot{z}_3 = i_{sd}^{\cdot} - i_{sd}^{\dot{*}} = \overline{a}_d i_{sd} + \omega_s i_{sq} + \overline{b}_d \varphi + \overline{d}_d V_{sd} + L_2 - i_{sd}^{\dot{*}},$$
$$\dot{z}_4 = i_{sq}^{\cdot} - i_{sq}^{\dot{*}} = \overline{a}_d i_{sq} - \omega_s i_{sd} + \overline{c}_d \omega \varphi + \overline{d}_d V_{sq} + L_3 - i_{sq}^{\dot{*}},$$
$$\dot{z}_5 = i_{sw}^{\cdot} - i_{sw}^{\dot{*}} = \overline{a}_w i_{sw} + \overline{d}_w V_{sw} + L_4 - i_{sw}^{\dot{*}},$$
$$\dot{z}_6 = i_{su}^{\cdot} - i_{su}^{\dot{*}} = \overline{a}_w i_{su} + \overline{d}_w V_{su} + L_5 - i_{su}^{\dot{*}}. \qquad (32)$$

By setting (32) in (5)–(7), the derivatives S_3, S_4, S_5, and S_6 are obtained as follows:

$$\dot{S}_3 = h_3 \cdot \left(c_3 \dot{z}_3 + z_3\right),$$
$$\dot{S}_4 = h_4 \cdot \left(c_4 \dot{z}_4 + z_4\right),$$
$$\dot{S}_5 = h_5 \cdot \left(c_5 \dot{z}_5 + z_5\right), \qquad (33)$$
$$\dot{S}_6 = h_6 \cdot \left(c_6 \dot{z}_6 + z_6\right)$$

and

$$\dot{S}_3 = h_3 \cdot \left(c_3 \left(\overline{a}_d i_{sd} + \omega_s i_{sq} + \overline{b}_d \varphi + \overline{d}_d V_{sd} + L_2 - i_{sd}^{\dot{*}}\right) + z_3\right),$$
$$\dot{S}_4 = h_4 \cdot \left(c_4 \left(\overline{a}_d i_{sq} - \omega_s i_{sd} + \overline{c}_d \omega \varphi + \overline{d}_d V_{sq} + L_3 - i_{sq}^{\dot{*}}\right) + z_4\right),$$
$$\dot{S}_5 = h_5 \cdot \left(c_5 \left(\overline{a}_w i_{sw} + \overline{d}_w V_{sw} + L_4 - i_{sw}^{\dot{*}}\right) + z_5\right),$$
$$\dot{S}_6 = h_6 \cdot \left(c_6 \left(\overline{a}_w i_{su} + \overline{d}_w V_{su} + L_5 - i_{su}^{\dot{*}}\right) + z_6\right). \qquad (34)$$

The nominal (d, q, w, u) voltages axis can be evaluated by setting $\dot{S}_3 = \dot{S}_4 = \dot{S}_5 = \dot{S}_6 = 0$ without the application of model uncertainties $L_3 = L_4 = L_5 = L_6 = 0$ as follows:

$$V_{sdn}^* = -\left(c_3 \overline{d}_d\right)^{-1}$$
$$\left(\left(c_3 \overline{a}_d + 1\right)z_3 + c_3 \overline{a}_d i_{sd}^* + c_3 \omega_s i_{sq} + c_3 \overline{b}_d \varphi - c_3 i_{sd}^{\dot{*}}\right), \qquad (35)$$

$$V_{sqn}^* = -\left(c_4 \overline{d}_d\right)^{-1}$$
$$\left(\left(c_4 \overline{a}_d + 1\right)z_4 + c_4 \overline{a}_d i_{sq}^* - c_4 \omega_s i_{sd} + c_4 \overline{c}_d \omega \varphi - c_4 i_{sq}^{\dot{*}}\right), \qquad (36)$$

$$V_{swn}^* = -\left(c_5 \overline{d}_w\right)^{-1} \left(\left(c_5 \overline{a}_w + 1\right)z_5 + c_5 \overline{a}_w i_{sw}^* - c_5 i_{sw}^{\dot{*}}\right), \qquad (37)$$

$$V_{sun}^* = -\left(c_6 \overline{d}_u\right)^{-1} \left(\left(c_6 \overline{a}_w + 1\right)z_6 + c_6 \overline{a}_w i_{su}^* - c_6 i_{su}^{\dot{*}}\right). \qquad (38)$$

Similar to what is considered when designing the speed and flux controllers, a reaching controller is incorporated within the control part to endure uncertainties behind the sliding surface. Then, the reaching control is defined by

$$V_{sdr}^* = -\left(\overline{d}_d\right)^{-1} \cdot k_3 \mathrm{sign}\left(S_3\right),$$
$$V_{sqr}^* = -\left(\overline{d}_d\right)^{-1} \cdot k_4 \mathrm{sign}\left(S_4\right),$$
$$V_{swr}^* = -\left(\overline{b}_w\right)^{-1} \cdot k_5 \mathrm{sign}\left(S_5\right), \qquad (39)$$
$$V_{sur}^* = -\left(\overline{d}_w\right)^{-1} \cdot k_6 \mathrm{sign}\left(S_6\right),$$

where k_3, k_4, k_5, and k_6 are the switching factors. Thus, a relevant control of (d,q,w,u) current components taking into account the uncertainties and unmodeled dynamics can be formulated by

$$V_{sd}^* = V_{sdn}^* + V_{sdr}^*,$$
$$V_{sq}^* = V_{sqn}^* + V_{sqr}^*,$$
$$V_{sw}^* = V_{swn}^* + V_{swr}^*, \qquad (40)$$
$$V_{su}^* = V_{sun}^* + V_{sur}^*.$$

In conclusion, the command (d, q, w, u) voltages are given by

$$V_{sd}^* = -\left(c_3 \overline{d}_d\right)^{-1}\left(\left(c_3 \overline{a}_d + 1\right)z_3 + c_3 \overline{a}_d i_{sd}^* + c_3 \omega_s i_{sq} + c_3 \overline{b}_d \varphi - c_3 i_{sd}^{\dot{*}}\right) - \left(\overline{d}_d\right)^{-1} \cdot k_3 \text{sign}\left(S_3\right),$$

$$V_{sq}^* = -\left(c_4 \overline{d}_d\right)^{-1}\left(\left(c_4 \overline{a}_d + 1\right)z_4 + c_4 \overline{a}_d i_{sq}^* - c_4 \omega_s i_{sd} + c_4 \overline{c}_d \omega \varphi - c_4 i_{sq}^{\dot{*}}\right) - \left(\overline{d}_d\right)^{-1} \cdot k_4 \text{sign}\left(S_4\right),$$

$$V_{sw}^* = -\left(c_5 \overline{d}_w\right)^{-1}\left(\left(c_5 \overline{a}_w + 1\right)z_5 + c_5 \overline{a}_w i_{sw}^* - c_5 i_{sw}^{\dot{*}}\right) - \left(\overline{b}_w\right)^{-1} \cdot k_5 \text{sign}\left(S_5\right),$$

$$V_{su}^* = -\left(c_6 \overline{d}_u\right)^{-1}\left(\left(c_6 \overline{a}_w + 1\right)z_6 + c_6 \overline{a}_w i_{su}^* - c_6 i_{su}^{\dot{*}}\right) - \left(\overline{d}_w\right)^{-1} \cdot k_6 \text{sign}\left(S_6\right).$$

$$(41)$$

$$V = \left(\frac{1}{2}\right)\sum_1^6 S_k^2 = \left(\frac{1}{2}\right)\left(S_1^2 + S_2^2 + S_3^2 + S_4^2 + S_5^2 + S_6^2\right). \quad (42)$$

3.3. Stability Check.

To analyze the stability of current and speed regulation, one can contemplate the Lyapunov function V as given as follows:

The stability state is achieved from the Lyapunov stability approach as follows:

$$\dot{V} = \sum_1^6 S_k \dot{S}_k = S_1 \dot{S}_1 + S_2 \dot{S}_2 + S_3 \dot{S}_3 + S_4 \dot{S}_4 + S_5 \dot{S}_5 + S_6 \dot{S}_6$$

$$\leq -\sum_1^6 h_k c_k \alpha_k \left|S_k\right| = -h_1 c_1 \alpha_1 \left|S_1\right| - h_2 c_2 \alpha_2 \left|S_2\right| - h_3 c_3 \alpha_3 \left|S_3\right| - h_4 c_4 \alpha_4 \left|S_4\right| - h_5 c_5 \alpha_5 \left|S_5\right| - h_6 c_6 \alpha_6 \left|S_6\right|,$$

$$(43)$$

where $(\alpha_i, i = 1, 2, 3, 4, 5, 6)$ need to be selected as small positive constants. Then by replacing (22) with (18), it results in

$$\dot{S}_1 = h_1\left(c_1\left(\overline{a}_\omega \Omega + \overline{b}_\omega \varphi\left(i_{sqn} + i_{sqr}\right) + L_1 - \dot{\Omega}^*\right) + z_1\right)$$
$$= h_1\left(-c_1 k_1 \text{sign}\left(S_1\right) + c_1 L_1\right). \quad (44)$$

Substituting from (30) in (26), it yields

$$\dot{S}_2 = h_2\left(c_2\left(\overline{a}_\varphi\left(i_{sdn} + i_{sdr}\right) + \overline{b}_\varphi \varphi + L_6 - \dot{\varphi}^*\right) + z_2\right)$$
$$= h_2\left(-c_2 k_2 \text{sign}\left(S_2\right) + c_2 L_6\right). \quad (45)$$

By setting (41) in (34), one obtains

$$\dot{S}_3 = h_3\left(c_3\left(\overline{a}_d i_{sd} + \omega_s i_{sq} + \overline{b}_d \varphi + \overline{d}_d\left(V_{sdn} + V_{sdr}\right) + L_2 - i_{sd}^{\dot{*}}\right) + z_3\right),$$

$$\dot{S}_4 = h_4\left(c_4\left(\overline{a}_d i_{sq} - \omega_s i_{sd} + \overline{c}_d \omega \varphi + \overline{d}_d\left(V_{sqn} + V_{sqr}\right) + L_3 - i_{sq}^{\dot{*}}\right) + z_4\right),$$

$$\dot{S}_5 = h_5\left(c_5\left(\overline{a}_w i_{sw} + \overline{d}_w\left(V_{swn} + V_{swr}\right) + L_4 - i_{sw}^{\dot{*}}\right) + z_5\right),$$

$$\dot{S}_6 = h_6\left(c_6\left(\overline{a}_w i_{su} + \overline{d}_w\left(V_{sun} + V_{sur}\right) + L_5 - i_{su}^{\dot{*}}\right) + z_6\right).$$

$$(46)$$

The relationships in (46) turn out to be as follows:

$$\dot{S}_3 = h_3\left(-c_3 k_3 \text{sign}\left(S_3\right) + c_3 L_2\right),$$
$$\dot{S}_4 = h_4\left(-c_4 k_4 \text{sign}\left(S_4\right) + c_4 L_3\right),$$
$$\dot{S}_5 = h_5\left(-c_5 k_5 \text{sign}\left(S_5\right) + c_5 L_4\right),$$
$$\dot{S}_6 = h_6\left(-c_6 k_6 \text{sign}\left(S_6\right) + c_6 L_5\right).$$

$$(47)$$

Substituting (44), (45), and (47) into (43), the expression of the Lyapunov function V can be determined as follows:

$$
\begin{aligned}
\dot{V} &= S_1\dot{S}_1 + S_2\dot{S}_2 + S_3\dot{S}_3 + S_4\dot{S}_4 + S_5\dot{S}_5 + S_6\dot{S}_6 \\
&= S_1 h_1\left(-c_1 k_1 \operatorname{sign}(S_1) + c_1 L_1\right) \\
&\quad + S_2 h_2\left(-c_2 k_2 \operatorname{sign}(S_2) + c_2 L_6\right) \\
&\quad + S_3 h_3\left(-c_3 k_3 \operatorname{sign}(S_3) + c_3 L_2\right) \\
&\quad + S_4 h_4\left(-c_4 k_4 \operatorname{sign}(S_4) + c_4 L_3\right) \\
&\quad + S_5 h_5\left(-c_5 k_5 \operatorname{sign}(S_5) + c_5 L_4\right) \\
&\quad + S_6 h_6\left(-c_6 k_6 \operatorname{sign}(S_6) + c_6 L_5\right).
\end{aligned}
\tag{48}
$$

Then using (48) and (43), the following condition is obtained:

$$
\begin{aligned}
\dot{V} &= S_1\dot{S}_1 + S_2\dot{S}_2 + S_3\dot{S}_3 + S_4\dot{S}_4 + S_5\dot{S}_5 + S_6\dot{S}_6 \\
&= S_1 h_1\left(-c_1 k_1 \operatorname{sign}(S_1) + c_1 L_1\right) \\
&\quad + S_2 h_2\left(-c_2 k_2 \operatorname{sign}(S_2) + c_2 L_6\right) + S_3 h_3\left(-c_3 k_3 \operatorname{sign}(S_3) + c_3 L_2\right) \\
&\quad + S_4 h_4\left(-c_4 k_4 \operatorname{sign}(S_4) + c_4 L_3\right) \\
&\quad + S_5 h_5\left(-c_5 k_5 \operatorname{sign}(S_5) + c_5 L_4\right) + S_6 h_6\left(-c_6 k_6 \operatorname{sign}(S_6) + c_6 L_5\right) \\
&\leq h_1 c_1 |S_1|\left(|L_1| - k_1\right) + h_2 c_2 |S_2|\left(|L_6| - k_2\right) \\
&\quad + h_3 c_3 |S_3|\left(|L_2| - k_3\right) + h_4 c_4 |S_4|\left(|L_3| - k_4\right) \\
&\quad + h_5 c_5 |S_5|\left(|L_4| - k_5\right) + h_6 c_6 |S_6|\left(|L_5| - k_6\right) \\
&\leq h_1 c_1 |S_1|\left(n_1 - k_1\right) + h_2 c_2 |S_2|\left(n_6 - k_2\right) \\
&\quad + h_3 c_3 |S_3|\left(n_2 - k_3\right) + h_4 c_4 |S_4|\left(n_3 - k_4\right) + \\
& h_5 c_5 |S_5|\left(n_4 - k_5\right) + h_6 c_6 |S_6|\left(n_5 - k_6\right) \leq - h_1 c_1 \alpha_1 |S_1| \\
&\quad - h_2 c_2 \alpha_2 |S_2| - h_3 c_3 \alpha_3 |S_3| - h_4 c_4 \alpha_4 |S_4| \\
&\quad - h_5 c_5 \alpha_5 |S_5| - h_6 c_6 \alpha_6 |S_6|.
\end{aligned}
\tag{49}
$$

Finally, the stability proof is obtained if the following conditions are obtained:

$$
\begin{cases}
|L_i| < n_i, & (i = 1, 2, 3, 4, 5, 6), \\
k_i \geq n_i + \alpha, & (i = 1, 2, 3, 4, 5, 6).
\end{cases}
\tag{50}
$$

3.4. Overall Formulation of the Proposed SO-SMC. As demonstrated in (50), the switching constants k_i are calculated on the basis of the magnitudes of the lumped uncertainties. Indeed, limiting the lumped uncertainties in real

applications cannot be usually ensured. Thus, to estimate the lumped uncertainties' upper bounds, an adaptively selected gain is proposed and represented by

$$
k_i = h_i c_i r_i \int_0^t |S_i(\tau)| \, \mathrm{d}\tau, \quad (i = 1, 2, 3, 4, 5, 6),
\tag{51}
$$

where r_i is a positive constant.

Based upon this hypothesis, the expressions of (20), (28), and (39) can be adjusted in the following manners:

$$
i_{sqr}^* = -\left(\overline{b}_w\right)^{-1} h_1 c_1 r_1 \int_0^t |S_1(\tau)| \, \mathrm{d}\tau,
\tag{52}
$$

$$
i_{sdr}^* = -\left(\overline{b}_\varphi\right)^{-1} h_2 c_2 r_2 \int_0^t |S_2(\tau)| \, \mathrm{d}\tau,
\tag{53}
$$

$$
\begin{cases}
V_{sdr}^* = -\left(\overline{d}_d\right)^{-1} h_3 c_3 r_3 \int_0^t |S_3(\tau)| \, \mathrm{d}\tau, \\[2mm]
V_{sqr}^* = -\left(\overline{d}_d\right)^{-1} h_4 c_4 r_4 \int_0^t |S_4(\tau)| \, \mathrm{d}\tau, \\[2mm]
V_{swr}^* = -\left(\overline{d}_w\right)^{-1} h_5 c_5 r_5 \int_0^t |S_5(\tau)| \, \mathrm{d}\tau, \\[2mm]
V_{sur}^* = -\left(\overline{d}_w\right)^{-1} h_6 c_6 r_6 \int_0^t |S_6(\tau)| \, \mathrm{d}\tau.
\end{cases}
\tag{54}
$$

To check the control stability of the speed, flux, and current, an adequate Lyapunov's formula is needed. The Lyapunov formula V is preferred as

$$
\begin{aligned}
V &= \frac{1}{2}\left(S_1^2 + S_2^2 + S_3^2 + S_4^2 + S_5^2 + S_6^2\right) \\
&\quad + \frac{1}{2}\left(\frac{1}{2r_1}\tilde{k}_1^2 + \frac{1}{2r_2}\tilde{k}_2^2 + \frac{1}{2r_3}\tilde{k}_3^2 + \frac{1}{2r_4}\tilde{k}_4^2 + \frac{1}{2r_5}\tilde{k}_5^2 + \frac{1}{2r_6}\tilde{k}_6^2\right),
\end{aligned}
\tag{55}
$$

where $\tilde{k}_i$ for $(i = 1, 2, 3, 4, 5, 6)$ is the estimated errors of k_i which are presented as follows: $\tilde{k}_i = k_i - \hat{k}_i$ for $(i = 1, 2, 3, 4, 5, 6)$, where $\hat{k}_i$ is the estimation of k_i. Differentiating formula (55), this results in

$$
\begin{aligned}
\dot{V} &= S_1\dot{S}_1 + S_2\dot{S}_2 + S_3\dot{S}_3 + S_4\dot{S}_4 + S_5\dot{S}_5 + S_6\dot{S}_6 \\
&\quad + \left(\frac{1}{2r_1}\right)\tilde{k}_1\dot{\tilde{k}}_1 + \left(\frac{1}{2r_2}\right)\tilde{k}_2\dot{\tilde{k}}_2 + \left(\frac{1}{2r_3}\right)\tilde{k}_3\dot{\tilde{k}}_3 \\
&\quad + \left(\frac{1}{2r_4}\right)\tilde{k}_4\dot{\tilde{k}}_4 + \left(\frac{1}{2r_5}\right)\tilde{k}_5\dot{\tilde{k}}_5 + \left(\frac{1}{2r_6}\right)\tilde{k}_6\dot{\tilde{k}}_6.
\end{aligned}
\tag{56}
$$

Using (22), (30), (31), and (33), the equality in (56) becomes

$$\dot{V} = h_1 c_1 S_1 \left(-k_1 \text{sign}\left(S_1\right) + L_1\right)$$
$$+ h_2 c_2 S_2 \left(-k_2 \text{sign}\left(S_2\right) + L_6\right)$$
$$+ h_3 c_3 S_3 \left(-k_3 \text{sign}\left(S_3\right) + L_2\right) + h_4 c_4 S_4 \left(-k_4 \text{sign}\left(S_4\right)$$
$$+ L_3\right) + h_5 c_5 S_5 \left(-k_5 \text{sign}\left(S_5\right) + L_4\right)$$
$$+ h_6 c_6 S_6 \left(-k_6 \text{sign}\left(S_6\right) + L_5\right)$$
$$+ \left(\frac{1}{2r_1}\right)\left(k_1 - \widehat{k}_1\right)\dot{k}_1 + \left(\frac{1}{2r_2}\right)\left(k_2 - \widehat{k}_2\right)\dot{k}_2$$
$$+ \left(\frac{1}{2r_3}\right)\left(k_3 - \widehat{k}_3\right)\dot{k}_3 + \left(\frac{1}{2r_4}\right)\left(k_4 - \widehat{k}_4\right)\dot{k}_4$$
$$+ \left(\frac{1}{2r_5}\right)\left(k_5 - \widehat{k}_5\right)\dot{k}_5 + \left(\frac{1}{2r_6}\right)\left(k_6 - \widehat{k}_6\right)\dot{k}_6.$$

$$(57)$$

Setting (57) into (43) and considering (50), the following is obtained:

$$\dot{V} < h_1 c_1 |S_1|\left(\left|L_1\right| - k_1\right) + h_2 c_2 |S_2|\left(\left|L_6\right| - k_2\right)$$
$$+ h_3 c_3 |S_3|\left(\left|L_2\right| - k_3\right) + h_4 c_4 |S_4|\left(\left|L_3\right| - k_4\right)$$
$$+ h_5 c_5 |S_5|\left(\left|L_4\right| - k_5\right) + h_6 c_6 |S_6|\left(\left|L_5\right| - k_6\right)$$
$$+ h_1 c_1 \left(k_1 - \widehat{k}_1\right)|S_1| + h_2 c_2 \left(k_2 - \widehat{k}_2\right)|S_2|$$
$$+ h_3 c_3 \left(k_3 - \widehat{k}_3\right)|S_3|$$
$$+ h_4 c_4 \left(k_4 - \widehat{k}_4\right)|S_4| + h_5 c_5 \left(k_5 - \widehat{k}_5\right)|S_5|$$
$$+ h_6 c_6 \left(k_6 - \widehat{k}_6\right)|S_6|$$
$$< h_1 c_1 |S_1|\left(n_1 - k_1\right) h_1 c_1 |S_1|\left(n_1 - k_1\right)$$
$$+ h_2 c_2 |S_2|\left(n_2 - k_2\right) + h_3 c_3 |S_3|\left(n_3 - k_3\right)$$
$$+ h_4 c_4 |S_4|\left(n_4 - k_4\right)+$$
$$h_5 c_5 |S_5|\left(n_5 - k_5\right) + h_6 c_6 |S_6|\left(n_6 - k_6\right)$$
$$+ h_1 c_1 \left(k_1 - \widehat{k}_1\right)|S_1| + h_2 c_2 \left(k_2 - \widehat{k}_2\right)|S_2|$$
$$+ h_3 c_3 \left(k_3 - \widehat{k}_3\right)|S_3| + h_4 c_4 \left(k_4 - \widehat{k}_4\right)|S_4|+$$
$$h_5 c_5 \left(k_5 - \widehat{k}_5\right)|S_5| + h_6 c_6 \left(k_6 - \widehat{k}_6\right)|S_6|$$
$$< -h_1 c_1 \alpha_1 |S_1| - h_2 c_2 \alpha_2 |S_2| - h_3 c_3 \alpha_3 |S_3|$$
$$- h_4 c_4 \alpha_4 |S_4| - h_5 c_5 \alpha_5 |S_5| - h_6 c_6 \alpha_6 |S_6|.$$

$$(58)$$

To maintain the stability of the control, the speed and current controllers should be selected as follows:

$$\widehat{k}_i \geq n_i + \alpha_i \, (i = 1, 2, 3, 4, 5, 6).$$

$$(59)$$

The control technique based on the sliding mode theory described in the previous paragraph provides a desired behavior of the closed-loop system. The actuators, on the
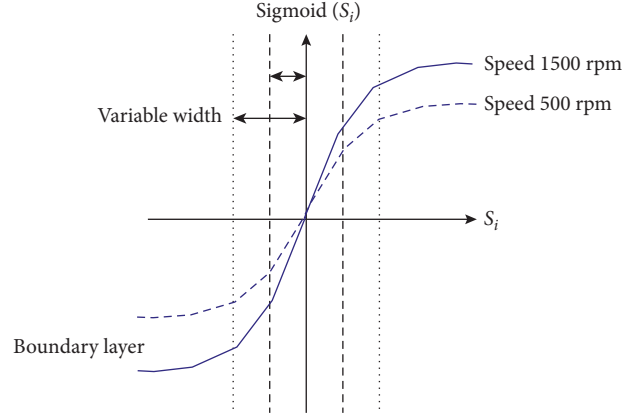

FIGURE 3: Variable boundary layers per the speed.

other hand, have an infinite commutation in the ideal scenario. As a result, no control member is capable of performing this operation. This results in high-frequency dynamics that are not accounted for in the system's modeling, resulting in the development of "reluctance" or "chatter," which is characterized by significant oscillations around the sliding surface.

To mitigate the problem impact, a zone around the sliding surface is designated, as illustrated in Figure 3, within which a less rigorous slip condition than the "sign" condition is enforced. Indeed, the previously employed *sign* function is replaced by a smoother function, which is the *Sigmoid* function expressed as

$$\text{Sigmoid}\left(S_i\right) = \frac{2}{1 + e^{-aS_i}} - 1.$$

$$(60)$$

4. General System Layout

The general system configuration of the designed SO-SMC is illustrated in Figure 4. The control measures the stator currents i_{abcde} and rotor speed ω, and then the angle θ_s is calculated and used for the coordinates transformation. The designed speed controller is used to develop the reference current i_{sq}^*, which is compared with the real current i_{sq} to get the current deviation z_3.

On the other hand, the designed flux controller is utilized to obtain the reference current i_{sd}^*, which is then subtracted from the real current i_{sd} to finally obtain the current error z_4. After that, both current errors z_3 and z_4 are fed to the designed current regulators to finally obtain the reference d-q voltages V_{sd}^* and V_{sq}^*. The reference currents i_{sw}^* and i_{su}^* are also compared with the actual currents i_{sw} and i_{su}, and the resultant errors are applied to their specified current regulators to obtain the reference voltage components V_{sw}^* and V_{su}^*. After obtaining all reference voltages, they are transformed using the angle θ_s to be applied to the PWM scheme, which is used to fire the gating of the inverter switches. All the necessary parameters for the designed adaptive SO-SMC are presented in Table 1. Meanwhile, Table 2 assigns the parameters of the FPIM.
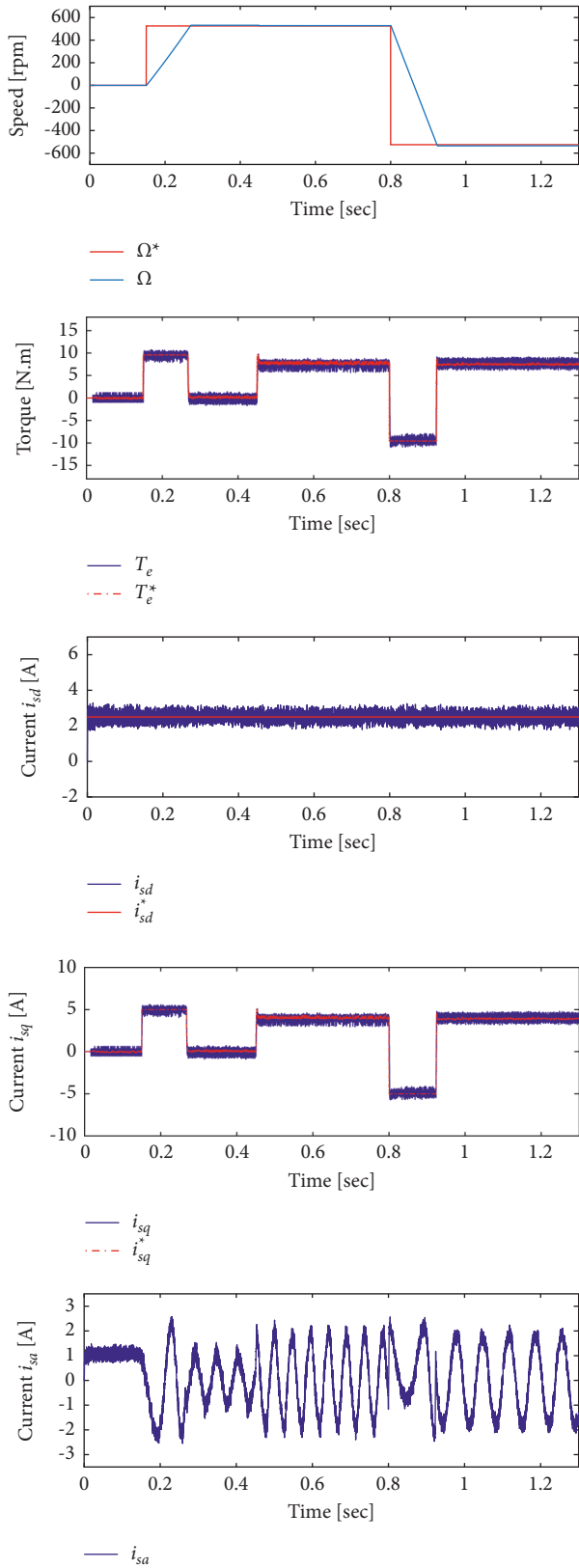
FIGURE 4: Control system layout for the SO-SMC.

TABLE 1: Parameters of the proposed SO-SMC.

Parameters	Value	Parameters	Value	Parameters	Value	Parameters	Value
h_1	0.0022	c_1	50	r_1	500	k_1	1200
h_2	0.1738	c_2	10	r_2	100	k_2	2000
h_3	0.0765	c_3	10	r_3	100	k_3	3000
h_4	0.0765	c_4	10	r_4	100	k_4	4000
h_5	0.04	c_5	10	r_5	100	k_5	2000
h_6	0.04	c_6	10	r_6	100	k_6	1000

TABLE 2: Parameters of five-phase IM.

Symbol	Value
R_s	10 Ω
R_r	6.3 Ω
L_s	0.46 H
L_r	0.46 H
M	0.42 H
L_{ls}	0.04 H
L^{lr}	0.04 H
J_m	0.01 kg·m^2
p	2
T_n	8.33 nm

5. Test Results

In order to prove and show the performance and effectiveness of the advanced SO-SMC technique, the control strategy is tested and evaluated under different operating conditions: the first test shown in Figure 5 is concerned to speed inversion with the application of the rated load toque

during a steady state. The operation consists of the following: starting using a zero reference speed, at instant $t = 0.15$ s, the reference speed variates to a value of 55 rad/s (525 rpm); after that, at instant $t = 0.45$ s, a full load torque is applied; and lastly, at time $t = 0.8$ s, the speed is reversed to a value of -525 rpm. One can observe that the speed control presents a precise reference tracking showing firstly a fast dynamic response without any detectable overshoot or undershoot. It can also be noticed that the designed adaptive SO-SMC has an agreeable performance from the point of view of settling time. It is also noticed that the designed SO-SMC displayed good performance from the point of view of disturbance. A slight speed dip is noticed after the load torque application; however, it does not hold any important effects on the control tracking performance. The stator currents i_{sd} and i_{sq} show appropriate tracking to their reference values. The component i_{sq} follows the torque change; meanwhile, the component i_{sd} is kept constant. The stator phase current "a" is also highly sinusoidal, even with a variable switching frequency.

FIGURE 5: Dynamic response: motor speed; electromagnetic torque; direct stator current; quadrature stator current; phase "a" stator current.
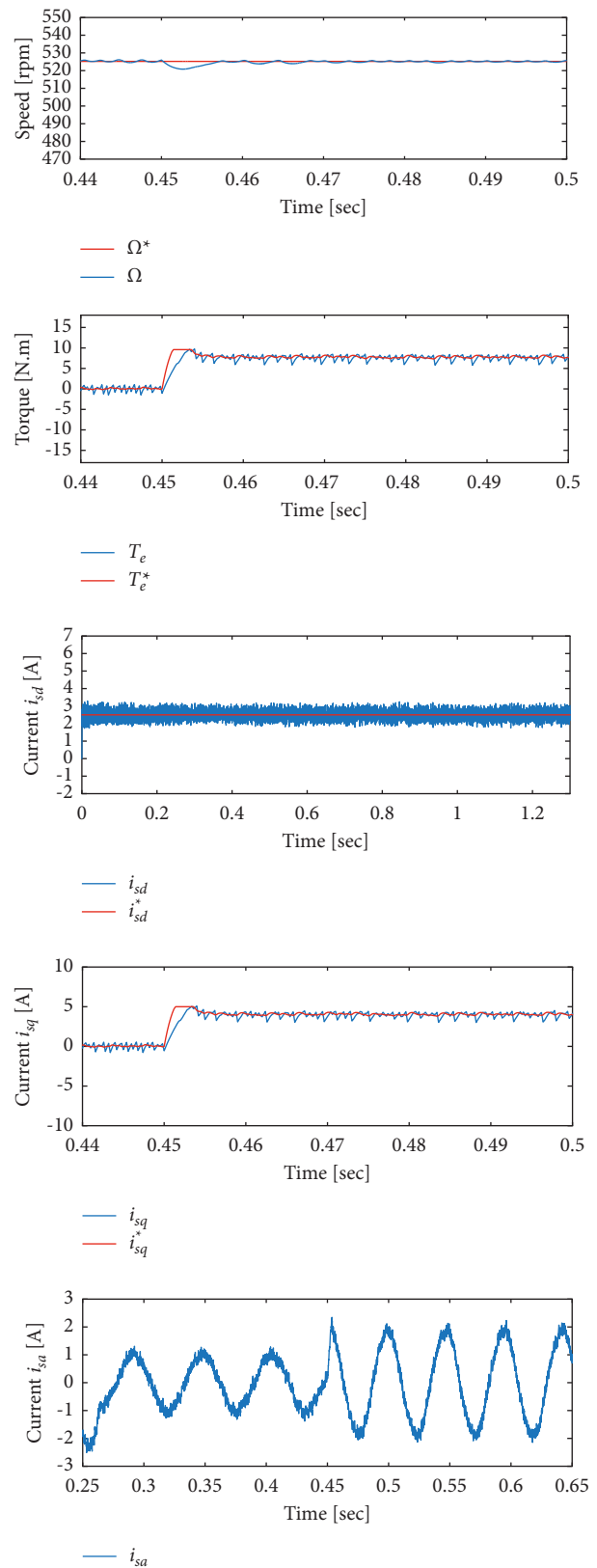
FIGURE 6: : Load torque effect-dynamic response: motor speed; electromagnetic torque; direct stator current; quadrature stator current; phase "a" stator current.
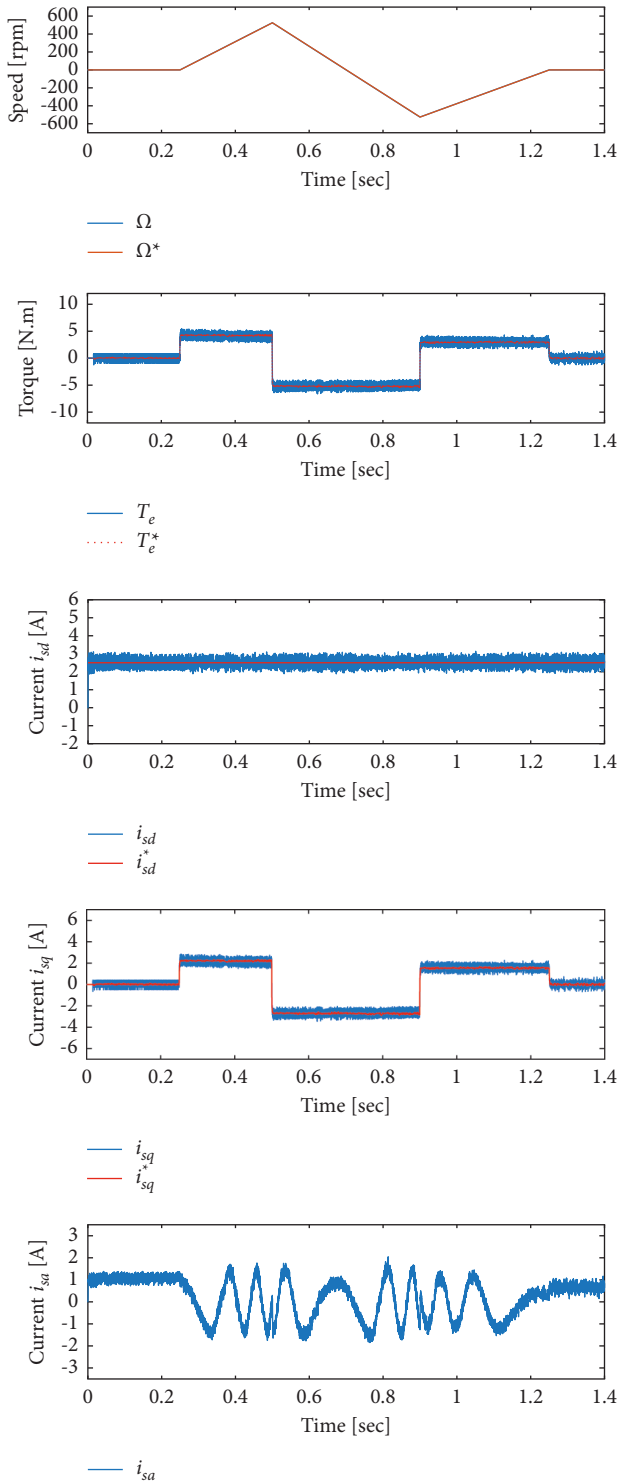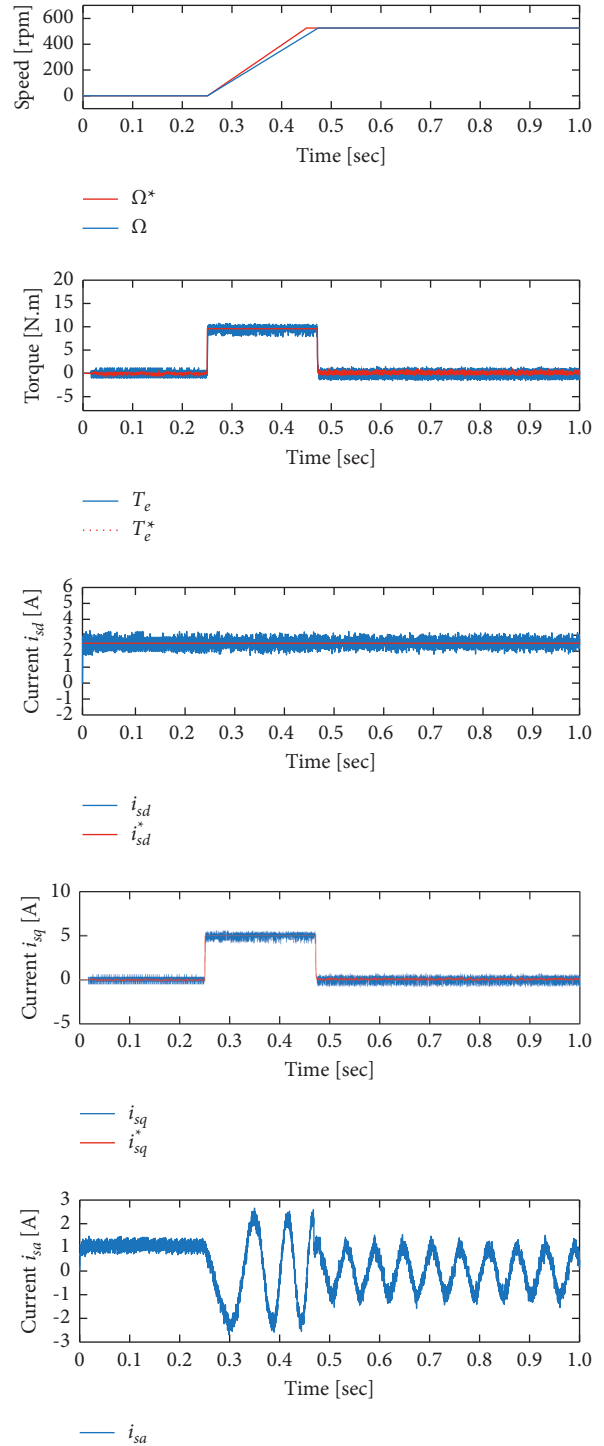
FIGURE 7: : Speed inversion effects: dynamic response: motor speed; electromagnetic torque; quadrature stator current; direct stator current; phase a stator current.

FIGURE 8: : Parameters variation effects: dynamic response: motor speed; electromagnetic torque; direct stator current; quadrature stator current; phase "a" stator current.

A zoomed view of the load impact is also shown in Figure 6, where at the time $t = 0.45$ s, the nominal load torque is applied. This result shows a fast disturbance rejection without steady-state error, which confirms the effectiveness of the designed SO-SMC.

Figure 7 highlights the response of the FPIM drive under triangular reference speed. The maneuver consists of the following: starting using a zero reference speed, at instant $t = 0.2$ s, the reference speed variates to a value of 525 rpm; after that, at instant $t = 0.4$ s, a reversal speed of -525 rpm is applied. Simulation results demonstrate that the envisaged
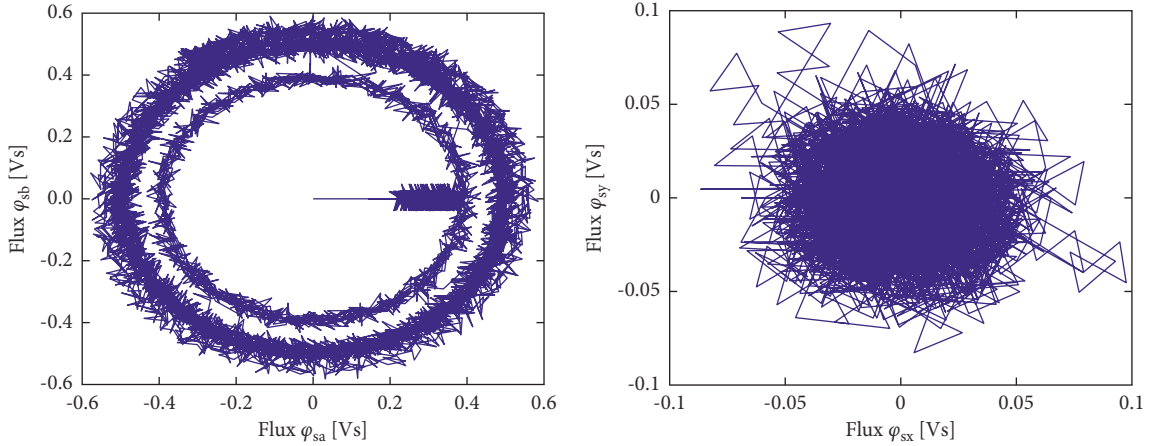
FIGURE 9: Stator flux loci for the full-load operation case with speed reversal.
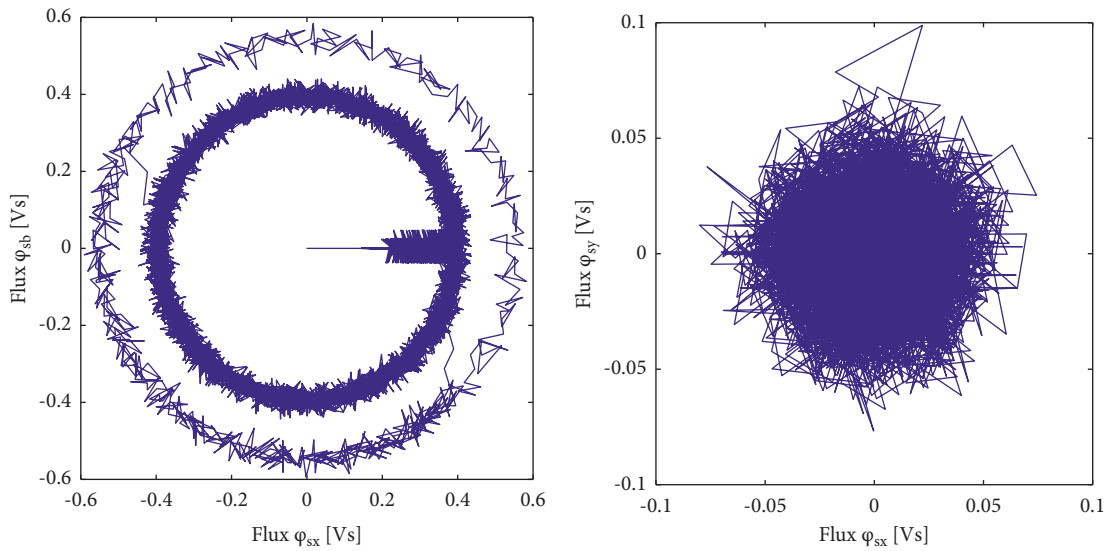
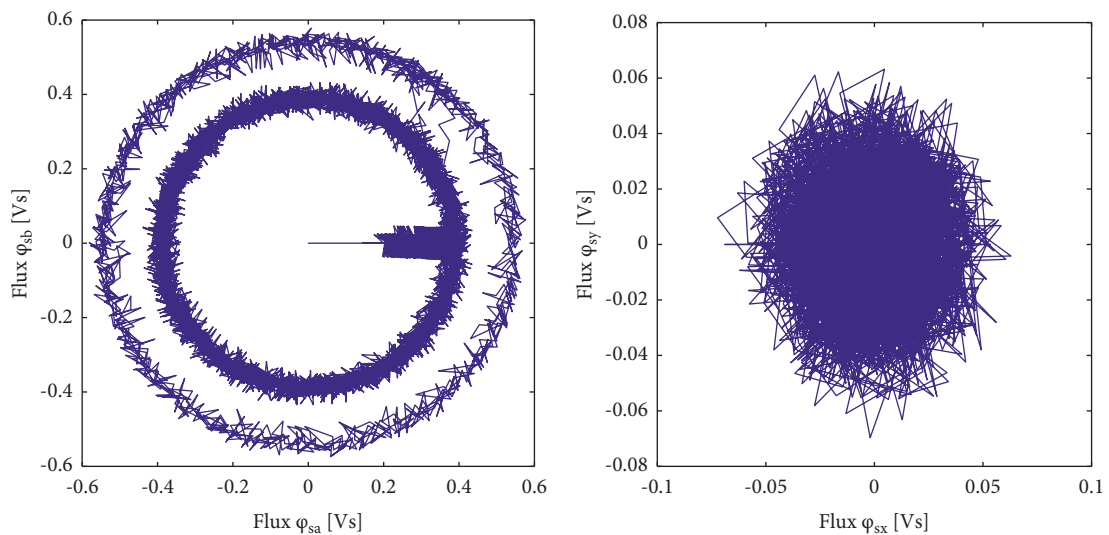FIGURE 10: Stator flux loci for the no-load load operation case with triangular speed reversal.

FIGURE 11: Stator flux loci for the no-load load operation case with ramp speed profile and parameters variation.
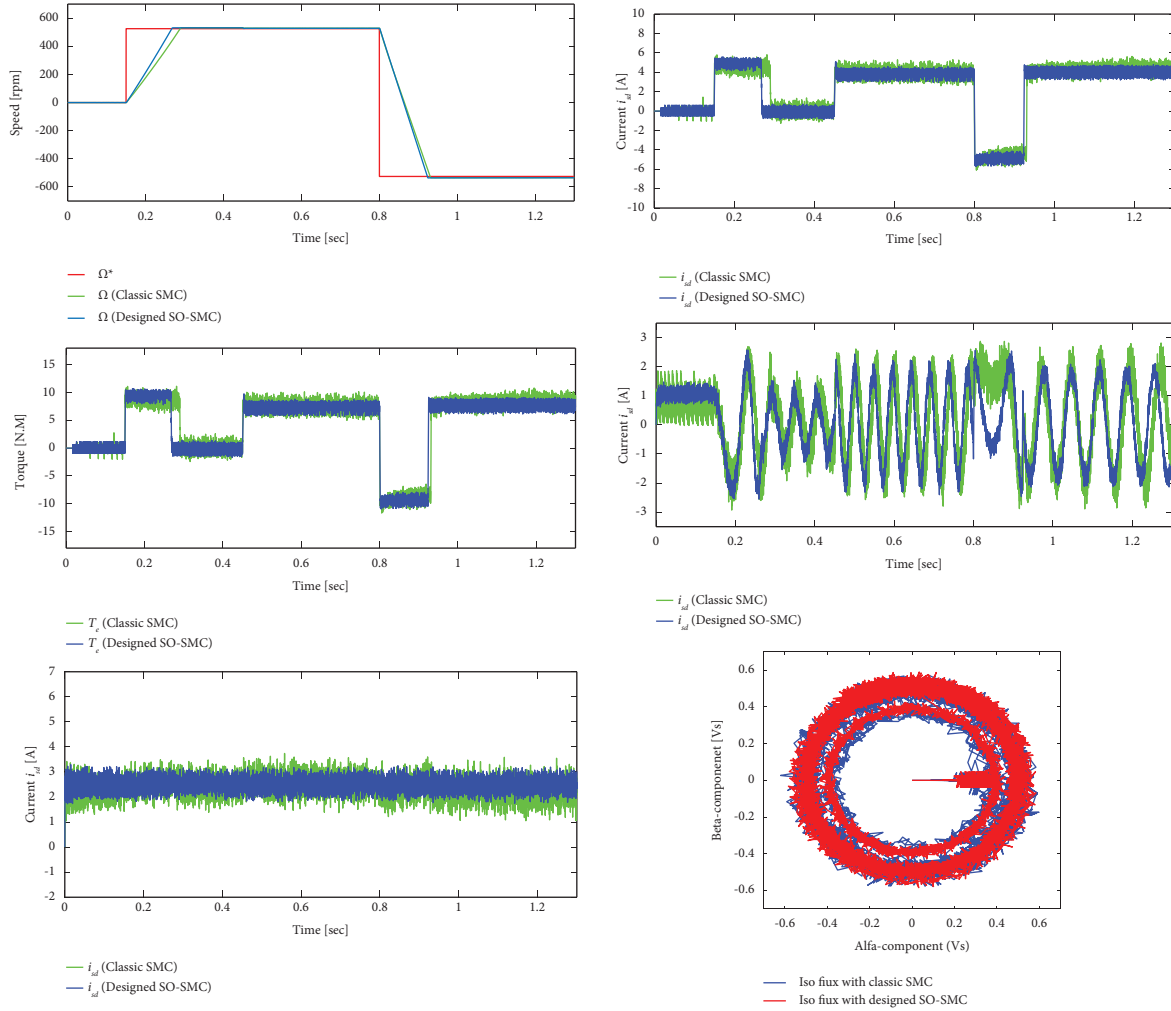
FIGURE 12: Dynamic response: motor speed; electromagnetic torque; direct stator current; quadrature stator current; phase "a" stator current and ISO stator flux for both classic SMC and designed SO-SMC for five-phase IM drive.

SO-SMC has significant performance, and this is illustrated through the fast and fast convergence of d-axis and q-axis current components to their reference values.

Moreover, the robustness of the designed SO-SMC faces the variation of parameters (in the current study, one will consider two mechanical parameters and one electrical parameter). The stator resistance variation is considered, in addition to a simultaneous variation of the friction coefficient and moment of inertia. A ramp speed variation is applied where the stator resistance is chosen at 200% of its nominal value. The speed, d-current, q-current, developed torque, and stator phase current are presented in Figure 8. One observes that the designed control is insensitive from the point of view of stator resistance variation, inertia moment, and friction coefficient. Good dynamic tracking is shown of the d–q currents components. It is pretended that the five-phase IM starts by applying 200% of the nominal values of both inertia moment and friction coefficient. Obtained results in Figure 8 approve the insensitivity of the proposed SO-SMC to the parameter variations; this is also accompanied by high dynamic performance during steady-state operation.

The ISO flux profiles for the ($\alpha\beta xy$) flux components are also presented for the three cases introduced above: loading case with speed reversal, no-load operation with triangular speed inverse variation, and ramp speed variation with parameters variation, respectively, in Figures 9–11. The shown flux loci exhibit circular waveforms for the three operating conditions, which confirms the effectiveness of the designed SO-SMC in keeping a uniform distribution of magnetic flux, whatever the operating conditions.

At last, a performance comparison test between the designed SO-SMC and classic SMC employed in the literature is performed. The test is carried out for a speed change of $(0 \longrightarrow 525 \longrightarrow -525)$ RPM at times of $(0 \longrightarrow 0.15 \longrightarrow 0.8)$ sec. The rated torque is applied to the motor at time $t = 0.45$ sec. This test is also carried out considering a variation in the stator resistance of 200% of its nominal value to test the robustness of the adopted system. As shown from the illustrated profiles in Figure 12, the actual speed is tracking appropriately its reference even under load disturbance and resistance variation, and this is ensured for both controllers (classic
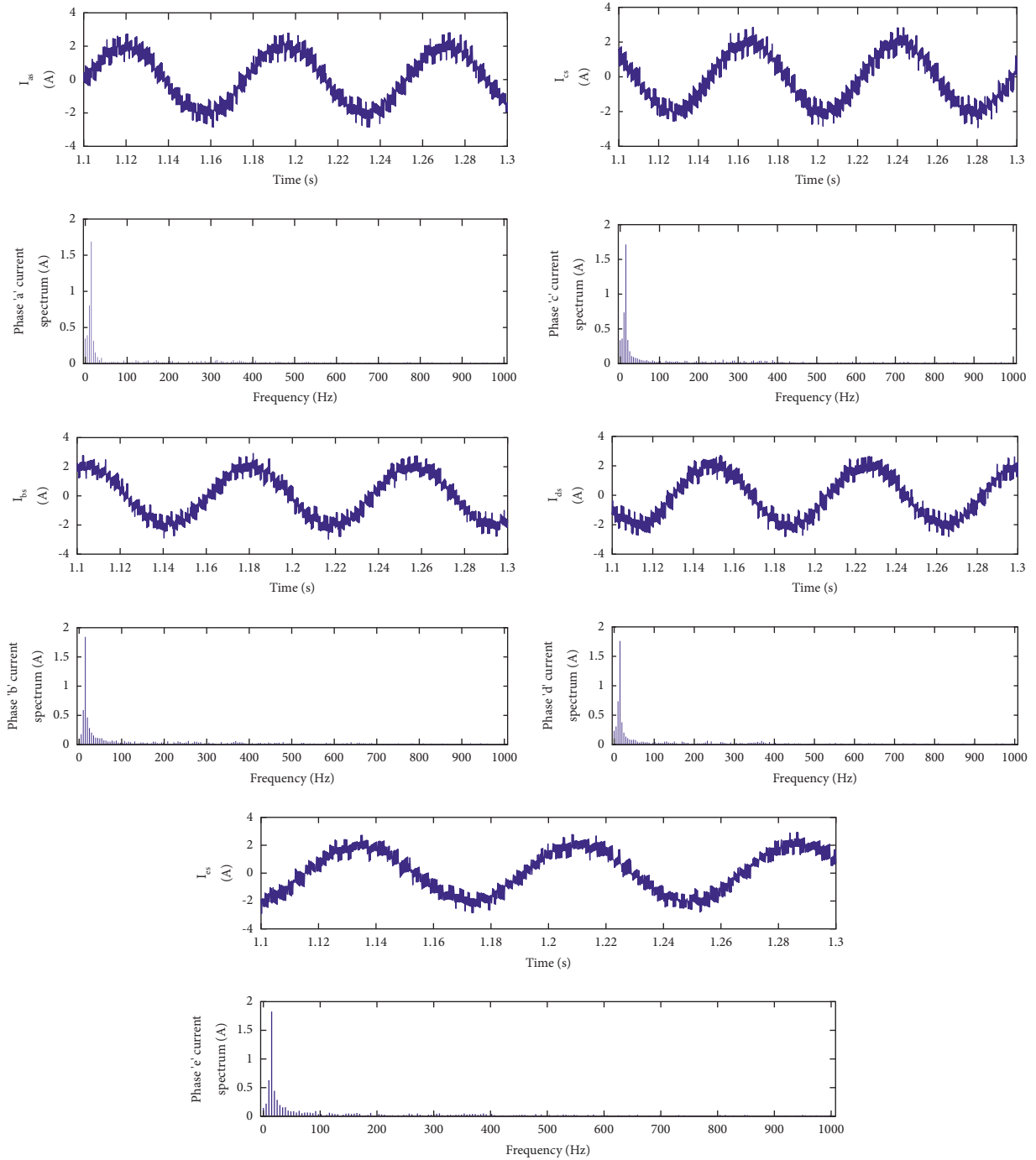
FIGURE 13: : Stator currents spectrum analysis under classic SMC.

SMC and designed SO-SMC). The developed torque also tracks precisely the desired value during the speed change for both controllers. The value of the d-axis stator current component is maintained effectively fixed at its reference value; meanwhile, the q-axis term effectively followed the change in the motor torque. On the other hand, it is very obvious from the comparison that the designed SO-SMC maintained a lower chattering rate causing a reduction in the accompanied ripples in comparison with the classic SMC, and this strongly validates the superiority of the designed SO-SMC over the classic SMC in maintaining high dynamic performance and at the same time limiting the chattering if possible. The superiority of the designed SO-SMC is also confirmed via analyzing the stator currents THD, and this is illustrated in Figures 13 and 14, which illustrate, respectively, the current spectrums for the two controllers (classic SMC and proposed SO-SMC). The THD percentage is effectively reduced under the proposed SO-SMC, and the values are numerically reported in Table 3.
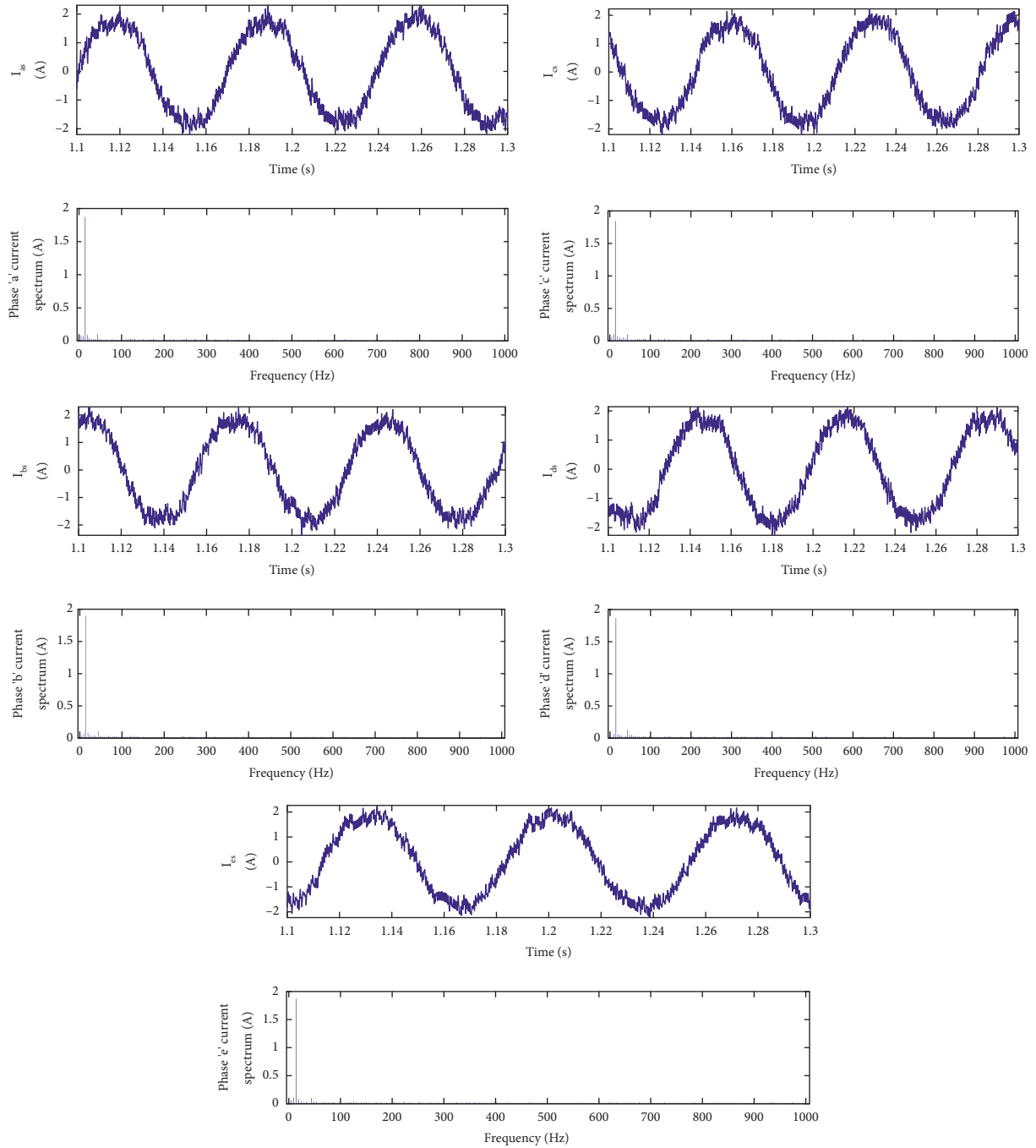
FIGURE 14: : Stator currents spectrum analysis under designed SO-SMC.

TABLE 3: Current THD analysis under the two control schemes.

Phase	Classic SMC	Designed SO-SMC
"A"	Fundamental (1.6878 A) THD (3.02%)	Fundamental (1.8716 A) THD (2.50%)
"B"	Fundamental (1.8430 A) THD (5.26%)	Fundamental (1.8960 A) THD (2.47%)
"C"	Fundamental (1.7149 A) THD (3.78%)	Fundamental (1.8448 A) THD (2.45%)
"d"	Fundamental (1.761 A) THD (4.09%)	Fundamental (1.8699 A) THD (2.87%)
"e"	Fundamental (1.8273 A) THD (4.94%)	Fundamental (1.8727 A) THD (2.36%)

6. Conclusion

The paper presented a detailed design for a robust adaptive second-order sliding mode control (SO-SMC) approach for a five-phase IM drive. The control design is performed and described in a systematic matter and accompanied by a system stability check to validate the effectiveness of the controller. Comprehensive evaluation tests for the five-phase IM drive are carried out under different operating conditions and considering system uncertainties as well. The obtained results reveal that the designed SO-SMC presents high system robustness against disturbance and parameter variation while keeping appropriate system dynamics and maintaining a circular distribution for the magnetic flux inside the machine. The calculated machine variables are also exhibiting high tracking precision to the reference signals with negligible steady-state deviation.

Data Availability

The data are available upon request from the first corresponding author Mahmoud A. Mossa.

Conflicts of Interest

The authors declare that they have no conflicts of interest.

References

[1] E. Levi, "Multiphase electric machines for variable-speed applications," *IEEE Transactions on Industrial Electronics*, vol. 55, no. 5, pp. 1893–1909, 2008.

[2] F. Locment, E. Semail, and X. Kestelyn, "Vectorial approach-based control of a seven-phase Axial flux machine designed for fault operation," *IEEE Transactions on Industrial Electronics*, vol. 55, no. 10, pp. 3682–3691, 2008.

[3] X. Huang, A. Goodman, C. Gerada, Y. Fang, and Q. Lu, "Design of a five-phase brushless DC motor for a safety critical aerospace application," *IEEE Transactions on Industrial Electronics*, vol. 59, no. 9, pp. 3532–3541, 2012.

[4] A. Mohammadpour and L. Parsa, "A unified fault-tolerant current control approach for five-phase PM motors with trapezoidal back EMF under different stator winding connections," *IEEE Transactions on Power Electronics*, vol. 28, no. 7, pp. 3517–3527, 2013.

[5] J.-R. Fu and T. A. Lipo, "Disturbance-free operation of a multiphase current-regulated motor drive with an opened phase," *IEEE Transactions on Industry Applications*, vol. 30, no. 5, pp. 1267–1274, 1994.

[6] I. González-Prieto, M. J. Duran, N. Rios-Garcia, F. Barrero, and C. Martín, "Open-switch fault detection in five-phase induction motor drives using model predictive control," *IEEE Transactions on Industrial Electronics*, vol. 65, no. 4, pp. 3045–3055, 2018.

[7] H. Guzman, F. Barrero, and M. J. Duran, "IGBT-gating failure effect on a fault-tolerant predictive current-controlled five-phase induction motor drive," *IEEE Transactions on Industrial Electronics*, vol. 62, no. 1, pp. 15–20, 2015.

[8] I. Gonzalez-Prieto, M. J. Duran, F. Barrero, M. Bermudez, and H. Guzmán, "Impact of postfault flux adaptation on six-phase induction motor drives with parallel converters," *IEEE Transactions on Power Electronics*, vol. 32, no. 1, pp. 515–528, 2017.

[9] H. Guzman, M. J. Duran, F. Barrero et al., "Comparative study of predictive and resonant controllers in fault-tolerant five-phase induction motor drives," *IEEE Transactions on Industrial Electronics*, vol. 63, no. 1, pp. 606–617, 2016.

[10] M. Bermudez, I. Gonzalez-Prieto, F. Barrero, H. Guzman, X. Kestelyn, and M. J. Duran, "An experimental assessment of open-phase fault-tolerant virtual-vector-based direct torque control in five-phase induction motor drives," *IEEE Transactions on Power Electronics*, vol. 33, no. 3, pp. 2774–2784, 2018.

[11] R. Karampuri, S. Jain, and V. T. Somasekhar, "Common-mode current elimination PWM strategy along with current ripple reduction for open-winding five-phase induction motor drive," *IEEE Transactions on Power Electronics*, vol. 34, no. 7, pp. 6659–6668, July 2019.

[12] H. Guzman, A. Iqbal, and F. Barrero, "Reduction of common-mode voltage using a simplified FSC-MPC for a five-phase induction motor drive," *Journal of Engineering*, vol. 2019, no. 17, pp. 3772–3777, 2019.

[13] J. Rodas, H. Guzmán, R. Gregor, and F. Barrero, "Model predictive current controller using Kalman filter for fault-tolerant five-phase wind energy conversion systems," in *Proceedings of the 2016 IEEE 7th International Symposium on Power Electronics for Distributed Generation Systems (PEDG)*, Vancouver, BC, Canada, 2016.

[14] J. Prieto, J. A. Riveros, and H. Guzmán, "Synchronized SVPWM techniques for five-phase drives," in *Proceedings of the 2017 IEEE 26th International Symposium on Industrial Electronics (ISIE)*, Edinburgh, UK, 2017.

[15] L. Zhang, Y. Fan, R. Cui, R. D. Lorenz, and M. Cheng, "Fault-Tolerant direct torque control of five-phase FTFSCW-IPM motor based on analogous three-phase SVPWM for electric vehicle applications," *IEEE Transactions on Vehicular Technology*, vol. 67, no. 2, pp. 910–919, 2018.

[16] Y. N. Tatte, M. V. Aware, J. K. Pandit, and R. Nemade, "Performance improvement of three-level five-phase inverter-fed DTC-controlled five-phase induction motor during low-speed operation," *IEEE Transactions on Industry Applications*, vol. 54, no. 3, pp. 2349–2357, 2018.

[17] A. I. H. Abu-Rub and J. Guzinski, *High Performance Control of Ac Drives with Matlab/Simulink Models*, Wiley, Hoboken, NJ, USA, 2012.

[18] Y. N. Tatte and M. V. Aware, "Direct torque control of five-phase induction motor with common-mode voltage and current harmonics reduction," *IEEE Transactions on Power Electronics*, vol. 32, no. 11, pp. 8644–8654, 2017.

[19] M. A Mossa, H. Echeikh, A. A. Z. Diab, H. Haes Alhelou, P. Siano, and P. Siano, "Comparative study of hysteresis controller, resonant controller and direct torque control of five-phase IM under open-phase fault operation," *Energies*, vol. 14, no. 5, 2021.

[20] B. Chikondra, U. R. Muduli, and R. K. Behera, "An improved open-phase fault-tolerant DTC technique for five-phase induction motor drive based on virtual vectors assessment," *IEEE Transactions on Industrial Electronics*, vol. 68, no. 6, pp. 4598–4609, 2021.

[21] M. Mossa and H. Echeikh, "A novel fault tolerant control approach based on backstepping controller for a five phase induction nmotor drive: experimental investigation," *ISA Transactions*, vol. 112, 2020.

[22] M. Bermudez, I. Gonzalez-Prieto, F. Barrero, H. Guzman, M. J. Duran, and X. Kestelyn, "Openphase fault-tolerant direct

torque control technique for five-phase induction motor drives," *IEEE Transactions on Industrial Electronics*, vol. 64, no. 2, pp. 902–911, 2017.

[23] M. A. Mossa, H. Echeikh, A. Iqbal, T. Duc Do, and A. S. Al-Sumaiti, "A novel sensorless control for multiphase induction motor drives based on singularly perturbed sliding mode observer-experimental validation," *Applied Sciences*, vol. 10, 2020.

[24] M. J. Duran and F. Barrero, "Recent advances in the design, modeling, and control of multiphase machines—part II," *IEEE Transactions on Industrial Electronics*, vol. 63, no. 1, pp. 459–468, 2016.

[25] F. Barrero and M. J. Duran, "Recent advances in the design, modeling, and control of multiphasemachines-part I," *IEEE Transactions on Industrial Electronics*, vol. 63, no. 1, pp. 449–458, 2016.

[26] H. Echeikh, R. Trabelsi, A. Iqbal, N. Bianchi, and M. F. Mimouni, "Comparative study betweenthe rotor flux oriented control and non-linear backstepping control of a five-phase induction motordrive-an experimental validation," *IET Power Electronics*, vol. 9, no. 13, pp. 2510–2521, 2016.

[27] M. A. Mossa, N. Vu Quynh, H. Echeikh, and T. D. Do, "Deadbeat-Based model predictive voltage control for a sensorless five-phase induction motor drive," *Mathematical Problems in Engineering*, vol. 2020, Article ID 4164526, 30 pages, 2020.

[28] L. Li, L. Sun, and S. Zhang, "Mean deviation coupling synchronous control formultiple motors via second-order adaptive sliding mode control," *ISA Transactions*, vol. 62, pp. 222–235, 2016.

[29] A. Saghafinia, H. W. Ping, M. N. Uddin, and K. S. Gaeid, "Adaptive fuzzy sliding-mode controlinto chattering-free im drive," *IEEE Transactions on Industry Applications*, vol. 51, no. 1, pp. 692–701, Jan2015.

[30] F. F. M. El-Sousy, "Adaptive dynamic sliding-mode control system using recurrent rbfn for highperformance induction motor servo drive," *IEEE Transactions on Industrial Informatics*, vol. 9, no. 4, pp. 1922–1936, 2013.

[31] L. B. Li, L.-L. Sun, S.-Z. Zhang, and Q. Q. Yang, "Speed tracking and synchronization of multiple motors using ring coupling control and adaptive sliding mode control," *ISA Transactions*, vol. 58, pp. 635–649, 2015.

[32] Z. Z., Y. Li Peng and Z. Liu, "Sensorless vector control of multiphase induction machine based on full-order observer and harmonic suppression," in *Proceedings of the IEEE 3rd International Future Energy Electronics Conference And ECCE Asia (IFEEC 2017-ECCE Asia)*, Kaohsiung, Taiwan, 2017.

[33] S.-Y. Kang and K.-B. Lee, "Improved switching selection for direct torque control of a five-phase induction motor," in *Proceedings of the IEEE Transportation Electrification Conference And Expo, Asia-Pacific (ITEC Asia-Pacific)*, Busan, Korea (South), 2016.

[34] S. Payami and R. K. Behera, "An improved dtc technique for low-speed operation of a five-phase induction motor," *IEEE Transactions on Industrial Electronics*, vol. 64, no. 5, pp. 3513–3523, 2017.

[35] Y. N. Tatte and M. V. Aware, "Torque ripple and harmonic current reduction in a three-level inverter-fed direct-torque-controlled five-phase induction motor," *IEEE Transactions on Industrial Electronics*, vol. 64, no. 7, pp. 5265–5275, 2017.

[36] S. Khadar, H. Abu-Rub, and A. Kouzou, "Sensorless field-oriented control for open-end winding five-phase induction motor with parameters estimation," *IEEE Open Journal of the Industrial Electronics Society*, vol. 2, pp. 266–279, 2021.

[37] H. Echeikh, R. Trabelsi, A. Iqbal, and M. F. Mimouni, "Adaptive direct torquecontrol using luenberger-sliding mode observer for online stator resistance estimation for five phase induction motor drives," *Electrical Engineering*, vol. 100, no. 3, pp. 1639–1649, 2017.

[38] M. Morawiec, P. Strankowski, A. Lewicki, J. Guziński, and F. Wilczyński, "Feedback control of multiphase induction machines with backstepping technique," *IEEE Transactions on Industrial Electronics*, vol. 67, no. 6, pp. 4305–4314, 2020.

[39] K. Saad, K. Abdellah, H. Ahmed, and A. Iqbal, "Investigation on svmbacksteppingsensorless control of five-phase open-end winding induction motor based on model reference adaptive system and parameter estimation," *Engineering Science and Technology, an International Journal*, vol. 22, no. 4, pp. 1013–1026, 2019.